ADVANCED FUNCTIONAL MATERIALS
www.afm-journal.de

Multifunctional Microstructured Surfaces by Microcontact Printing of Reactive Microgels

*Inga Litzen, Alexander Töpel, Martin Zenke, Antonio Sechi, and Andrij Pich**

Surface modification is an important tool to tailor the interactive properties of support materials to the desired application. It is commonly applied to design complex systems for applications in bio- or electro-technology. In this work, means of surface structuring and chemical modification are combined to create stable microgel patterned substrates, which can be post-modified with functional molecules. Poly(*N*-vinylcaprolactam-*co*-glycidyl methacrylate) (p(VCL-*co*-GMA)) microgels are used as functional colloidal inks to generate surface grafted patterns on glass by microcontact printing. This allows for the fabrication of microgel arrays with controlled geometries (line widths 10–50 µm and spacings 10–50 µm). Preliminary coupling tests in dispersion are conducted to determine the ideal reaction conditions for post-modifying the printed structures with the fluorescent model-compound Cyanine3 amine (Cy3 amine) and demonstrating the successful modification with a cell-adhesive peptide sequence. Surface-chemical gradients with variable profiles are created on the microgel patterns by dip-coating the fluorescent model compound Cy3 amine. Eventually, patterned substrates are applied in tissue culture experiments with NIH-3T3 cells, where peptide-modified surfaces enable increased control over cell adhesion and motility.

1. Introduction

Surface modifications with functional polymers allow for tailoring of material properties for a large variety of applications. Specifically, non-stick[1] self-cleaning[2] or anti-fouling properties[3] are often required to design complex systems.[4] Current methods of surface modification often lack flexibility regarding the manipulation of multiple surface properties at once. This however, is of high interest for tissue culture applications, since cells respond to a multitude of different cues, e.g., structural, chemical and mechanical properties.[5] Surface chemical gradients caused movement of droplets,[6] but gradients of growth factors or cell adhesive peptides were found to have a significant influence on cell fate and behavior, which was verified by observing a variety of parameters. DeLong et al. observed a 30% increased migration distance for fibroblasts moving up a RGDS gradient compared to motion toward lower surface concentration.[7] Ender et al. found that RGD gradients on amyloid-like fibrils (p(VCL-*co*-GMA)) lead to a more than twofold increase in cell number when comparing both ends of the gradient.[8] Laminin derived peptide gradients with varying steepness were created by Motta et al.[9] They observed that RGD gradients showed the most visible difference in Schwann cell proliferation when comparing high and low concentrations. YGSR however, more efficiently promotes alignment of the actin cytoskeleton. They were also able to quantify a chemotaxis index, which is the distance travelled by each cell in the direction of the gradient divided by the total path length, and this proved to be higher for steeper gradients. Lagunas et al. found that the number and length of focal contacts as well as the cell projected area increases toward higher RGD concentration.[10]

The use of structured substrates is an established strategy in tissue culture to study influences on cell behavior.[4,11] Since Wilbur et al. developed the microcontact printing technique,[12] it has evolved from direct patterning of biomolecules like fibronectin,[13] laminin[14] or poly(lysine)[15] to more complex biohybrid surfaces.[16] Knowledge from such investigations is useful to develop new strategies for wound healing and tissue regeneration applications. Since the extracellular matrix not only provides cells with structural but also mechanical support and allows for the transport of nutrients and signaling molecules, it is

I. Litzen, A. Töpel, A. Pich
Functional and Interactive Polymers
Institute of Technical and Macromolecular Chemistry
RWTH Aachen University
Worringerweg 2, 52074 Aachen, Germany
E-mail: pich@dwi.rwth-aachen.de
I. Litzen, A. Töpel, A. Pich
DWI – Leibniz-Institute for Interactive Materials e.V.
Forckenbeckstraße 50, 52074 Aachen, Germany
M. Zenke[+], A. Sechi[+]
Department of Cell Biology
Institute of Biomedical Engineering
RWTH Aachen University
Pauwelsstr. 30, 52075 Aachen, Germany

The ORCID identification number(s) for the author(s) of this article can be found under https://doi.org/10.1002/adfm.202516135

[+]Present address: Department of Medicine IV, Hematology, Oncology, Hemostaseology, and Stem Cell Transplantation, Faculty of Medicine, RWTH Aachen University, Pauwelsstr. 19, 52074 Aachen, Germany

DOI: 10.1002/adfm.202516135

desirable to develop surfaces which enable the adaption of multiple characteristics.[17] Microgels are interesting candidates for such applications since they are soft, porous colloids, which swell in aqueous media.[18] Their size, mechanical properties and morphology can be readily adapted during synthesis.[18] They adhere well to surfaces due to their flexible network structure[19] and can even be covalently bound if they contain functional groups.[20] Microgels are also modified and loaded with a variety of biomolecules.[21,22] Their potential application as drug-carriers,[23] sensors[24] but also coatings with enhanced biocompatibility[25] have been investigated. In cell culture, coatings of microgel layers have been studied as prospects for the triggered release of cell sheets.[26] Patterns of poly(*N*-isopropylacrylamide) and poly(*N*-isopropylacrylamide-*co*-acrylic-acid) produced via ink-jet spotting have been used as cell culture substrates by Uhlig et al. in 2016.[27] Xia et al. produced patterns of poly(*N*-isopropylacrylamide-*co*-styrene) microgels to co-culture different cell types and harvest them upon temperature switching.[28]

Sechi and Riegert et al. extensively studied the behavior of cells on linear poly(*N*-isopropylacrylamide) (pNIPAm) microgel arrays.[29,30] The patterns were generated by imprinting the structure of PDMS wrinkles with spacing lengths from 300–1600 nm.[30] Studied parameters include cell morphology, cytoskeleton alignment and directionality of cell motion and focal adhesion kinetics. Seeded on the microgel arrays, cells exhibited orientation of actin cytoskeleton and focal adhesions along the topological features of the substrates. On the control substrates however, namely glass and microgel films, cells were spread out and their actin cytoskeleton and focal adhesions were randomly oriented. The speed of cell movement proved to depend on the array spacing and could be slowed down or even increased compared to the bare glass reference. Microgels with higher crosslinker content, which are more rigid, reduced focal adhesion turnover. The system was designed to precisely control cell behavior and study complex tissue processes. Even though it offers some flexibility regarding the scale of the topological features in the range of several hundred nanometers, it is limited due to the array fabrication method via PDMS wrinkles. More precisely, that means only line patterns in the size range below 2 µm are accessible. Furthermore, neither the microgels themselves nor functional biomolecule coatings can be stably bound. Instead, the microgels themselves and a functional coating were immobilized via adhesion forces.[29,30]

Peng et al. adapted the microcontact printing method for reverse structuring of microgels.[31] Removal of microgels from a spin-coated monolayer was achieved with a cooled PDMS stamp to create the negative pattern. Since the used microgels contained the hydrophobic comonomer *tert*-b–utyl acrylate, their volume phase transition temperature was lowered compared to pure pNIPAm microgels. It is suggested that microgels transfer onto the water layer on the cooled PDMS stamp, which condenses upon exposure to ambient conditions. Various shapes, including lines, spots and hexagons ranging from 10–200 µm in size, were transferred.[31]

Even though different polymer and microgel patterned substrates have successfully been applied in tissue culture, one major drawback of the so-far employed systems is their limited stability and flexibility regarding structure and reactivity. The use of microcontact printing enables maximum flexibility in creating diverse patterns. Patterning substrates via microcontact printing allows for a relatively flexible choice of dimensions and patterns. This is a clear advantage compared to self-assembly techniques or printing with nano-wrinkles, which are techniques previously used to study cell growth and movement on microgel structured surfaces. When combined with the application of reactive microgels, this approach establishes a powerful platform for developing complex and stable cell culture substrates. Furthermore, post-modification of microgels is achievable under mild conditions avoiding potentially extreme pH levels or high temperatures opposed to direct incorporation during synthesis. Hence, post-modification of microgels is well suited for the incorporation of sensitive biomolecules, such as the peptide recognition motif RGD.

As described above, several microgel-based cell culture substrates have been described before. However, current systems are lacking flexibility regarding structural features and chemical functionalities, which can be applied with the same technique as well as stability through stable binding to the surface. To model complex tissue processes involving multiple cell types, it is also necessary to provide substrates adapted to their specific needs with good long-term stability. To the best of our knowledge, no material combining all these features has been reported in the literature to this day. In this work, core-shell poly(N-vinylcaprolactam-*co*-glycidyl methacrylate) microgels are employed as reactive building blocks to create patterned surfaces via microcontact printing. With this method, there is great freedom in the choice of shape or pattern in the size range from 0.5–200 µm. As a proof of principle, we generate stripe patterns between 10 and 50 µm, which is the size range of cells. The applied p(VCL-*co*-GMA) microgels with core-shell morphology p(VCL-*co*-10mol%GMA-shell) have especially been proven to be suitable for post-modification, as shown by Häntzschel[32] and Gau[21] since the pendant epoxy groups can undergo ring-opening click reactions with nucleophiles such as primary amines and thiols.[33] First, this reactivity is employed to achieve stable binding on amine-functionalized glass. Second, the reactive epoxy groups enable the formation of surface chemical gradients with an amine functionalized fluorescent dye, which is explored as a proof of concept. Employing NIH-3T3 cells reveals a measurable response to post-modification with a reactive RGD-based peptide by an increased number and overall size area of focal adhesions. Furthermore, RGD modification promotes alignment along the surface topology.

2. Results and Discussion

A schematic overview of the experimental work is given in **Figure 1**. First, p(VCL-*co*-10mol%GMA-shell) microgels were transferred onto (3-aminopropyl)triethoxysilane (APTES) functionalized glass via microcontact printing. The patterns are determined by design (stripe patterns with varying width and gap sizes) of the PDMS stamp. A reaction between surface amine groups and the microgels' epoxy moieties ensures stable binding. The stripe-patterned substrates could then be post-modified through reactions with the model compound Cyanine 3 amine

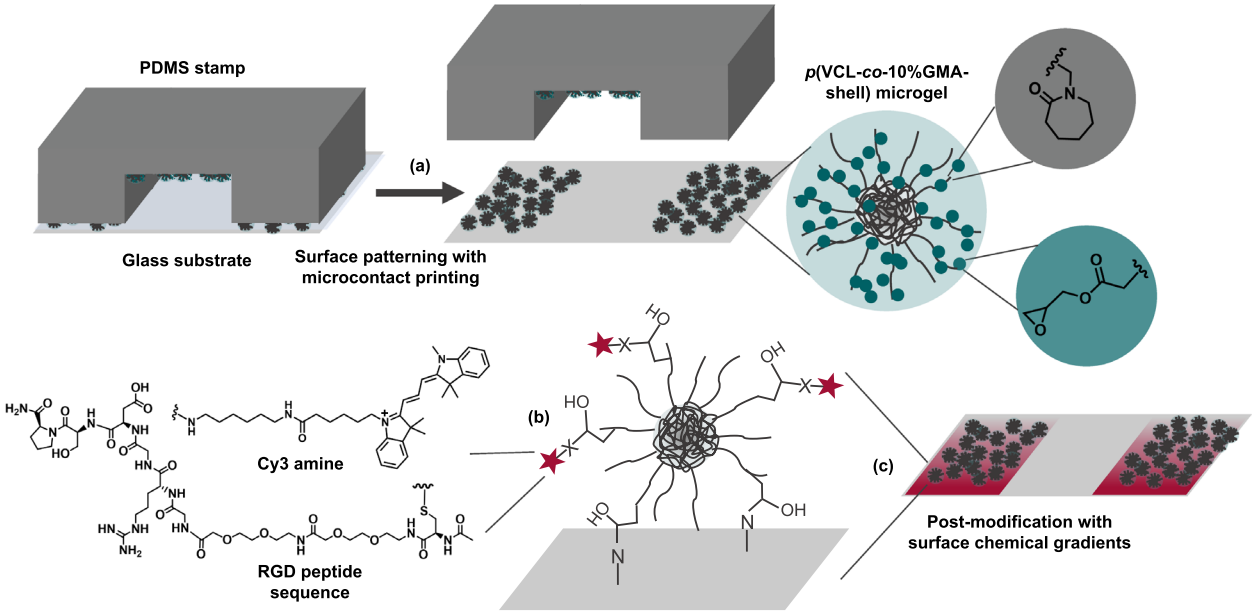

Figure 1. Generation of stable, functional, structured microgel-based substrates for tissue culture applications. a) Microgel-loaded PDMS stamps are used to transfer the patterns onto the glass substrate base. b) Stable binding to a functional surface is facilitated through an epoxy/amine reaction. Reactive post-modification facilitates the immobilization of cell adhesive peptides like RGD at a cell contacting interface. c) Surface chemical gradients, which can be easily visualized, are generated by post-modification with Cy3 amine.

(Cy3 amine) or a thiol-functionalized RGD-peptide sequence in a later step.

2.1. Microgel Characterization

The synthesized microgel exhibits temperature-responsive behavior in the analysis with dynamic light scattering (DLS) and electrophoretic light scattering (ELS). **Figure 2**a shows that the hydrodynamic diameter (D_h) is decreasing with increasing temperature. A biphasic phase transition hinting at a core-shell morphology is indicated by the dent at ≈20 °C. The temperature-responsive behavior is reversible since data for both heating and cooling cycle match within the error range. The polydispersity (Figure 2b) of the microgels is relatively high with values up to 0.37 at low temperatures. This is due to the fact that the microgels are not completely spherical but rather contain globular domains of the GMA comonomer in their shells which is in good agreement with literature[21] and furthermore confirmed with AFM imaging (Figure 2d,e). A core-shell morphology is indicated since the images show microgels with a dense center, exhibiting a larger height than the surrounding domains (Figure 2f). The synthesized microgels exhibit a positive zetapotential (Figure 2c) due to positively charged moieties from the initiator. The zetapotential increases with temperature due to temperature-induced shrinking of the polymer-structure.

2.2. Surface-Binding of Microgels Enhances Stability of Micropatterns

Microcontact printing allows for a flexible choice of dimensions and patterns. This is a clear advantage compared to self-assembly techniques or printing with nano-wrinkles, which are techniques that were previously used to study the growth and motion of cells on microgel-structured surfaces. A schematic overview of the printing process is presented in Scheme 1.

In this work, line patterns with dimensions between 10 and 50 µm were applied. This size range was chosen to accommodate various types of human and murine cell lines, including NIH-3T3 cells, which clearly distinguishes this work from previous systems employing line patterns in the range below 2 µm.[29,30] We expected that individual cells adhesion would take place on distinct micrometer-sized stripes rather than multiple nanometer-sized adjacent lines and points of adhesion can distinguished from the ones on the substrate background more easily.

Figure 3 shows representative microscopy data for 50 µm microgel stripe structures with a 10 µm spacer. Light microscopy images demonstrate an accurate transfer of the broad dimension of the stamp over a larger area. Atomic force microscopy reveals an equal distribution of microgels over the stripes. Only few microgels particles were found in the spacer area. The expected horizontal dimensions for these prints are also confirmed by the given height profiles. The step height is in good agreement with the particle height of individual microgels used in these experiments (Figure 2f). Stripe patterns with different widths and gap sizes ranging from 10–50 µm in size could also be demonstrated.

The stability of topological features is extremely important to allow for application in long-term studies, e.g., p when exploring tissue regeneration. This is why many studies employ surface grafted polymers.[34,35] However, this often involves complicated multi-step protocols and thorough removal of potentially cytotoxic monomers and non-grafted polymers.[16] The stability of microgel structures on amine-modified and

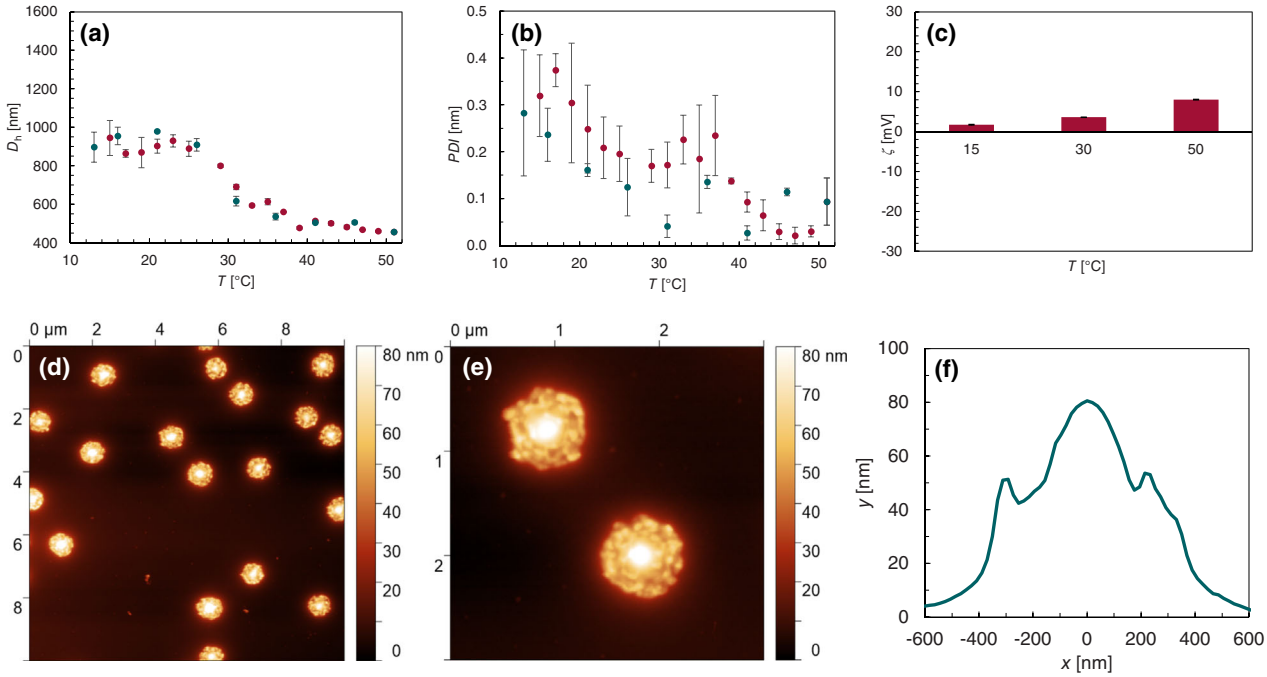

Figure 2. Temperature-dependent DLS and ELS measurements of p(VCL-*co*-10mol%GMA-shell) microgel in water and atomic force microscopy results of microgels spincoated on an Si wafer. a) Hydrodynamic diameter (D_h), b) polydispersity (*PDI*), and c) zeta potential (ζ) of the dispersed sample were measured between 15 and 50 °C. The data points for the heating cycle are shown in red, data for the following cooling cycle in turquoise. Error bars: mean ± standard deviation ($n = 3$). d) shows a 10 × 10 µm scan, e) a 3 × 3 µm scan and f) a height profile of a microgel with average height and diameter. Imaging confirms core-shell structure of the microgel.

plasma-activated glass were compared by treating both samples equally with different methods to prove the binding of epoxy groups to the amino-silane treated surface. Samples were exposed to media, i.e., surfactant solution (CTAB) and organic solvent (THF), which were chosen to aid the solvation of microgels, especially one with hydrophobic domains. Thus, the adhesion could be overcome for non-covalently bound microgels leading to detachment from the surface and eventually destruction of the pattern. However, light microscopy images of the dried substrates reveal that immersion in aqueous CTAB solution (**Figure** 4a,e) or THF (Figure 4b,f) does not cause significant detachment of the microgels from the substrate since the patterns remain intact. It has to be noted, however, that the lines themselves appear to be fainter, in some cases with frayed edges and small defects, for prints on plasma-treated glass compared to the amine-modified glass suggesting microgel detachment. As it can be seen from the AFM images of individual microgels (Figure 2e), the colloids have a low height to diameter ratio in the dry state at the surface, underlining the positive interaction with the underlying surface. This might explain why even microgels, which are not covalently bound to the substrates strongly adhere and patterns remain recognizable after exposure to CTAB solution and THF for both substrate types. However, this adhesion can be decreased if the temperature of the medium is lowered below the volume phase transition temperature causing the microgel to swell more, as shown in the temperature-dependent measurements of the hydrodynamic diameter (Figure 2a). This effect has in some cases been harnessed for the controlled release of adherent cells from microgel- or polymer-based tissue culture substrates.[27,28,34,35] Microgel patterns on plasma-treated glass, which have been exposed to cold water repeatedly under gentle agitation (Figure 4c), appear more faded when compared to prints on amine-modified glass (Figure 4g). In our case, it is additionally necessary to fully disrupt the adhesion between microgels and the underlying substrate with ultrasound to see a clear difference between covalently attached and adhering microgels. This might be explained by the shell-located hydrophobic GMA domains, which respond less to swelling upon cooling than the more hydrophilic VCL-core. Only the print on plasma-treated, non-silanized glass, which was washed with cold water and treated with ultrasound showed significant detachment of the microgel. In Figure 4d, the pattern becomes unrecognizable. On the respective amine-functionalized glass (Figure 4h), the structures remain largely intact even though the lines show a few defects. As findings by Izak-Nau et al. suggest, shear forces arising from ultrasound may disrupt bonds especially in the usually loosely crosslinked microgel shell.[36]

In conclusion, tests comparing the stability of patterns of p(VCL-*co*-10%GMA-shell) microgels on amine-modified and a plasma-treated glass reference strongly indicate that microgels containing epoxy moieties are indeed bound to the modified glass. Such stability could not be achieved with previously established systems of plasma activated pNIPAm-nanogel patterns.[30]

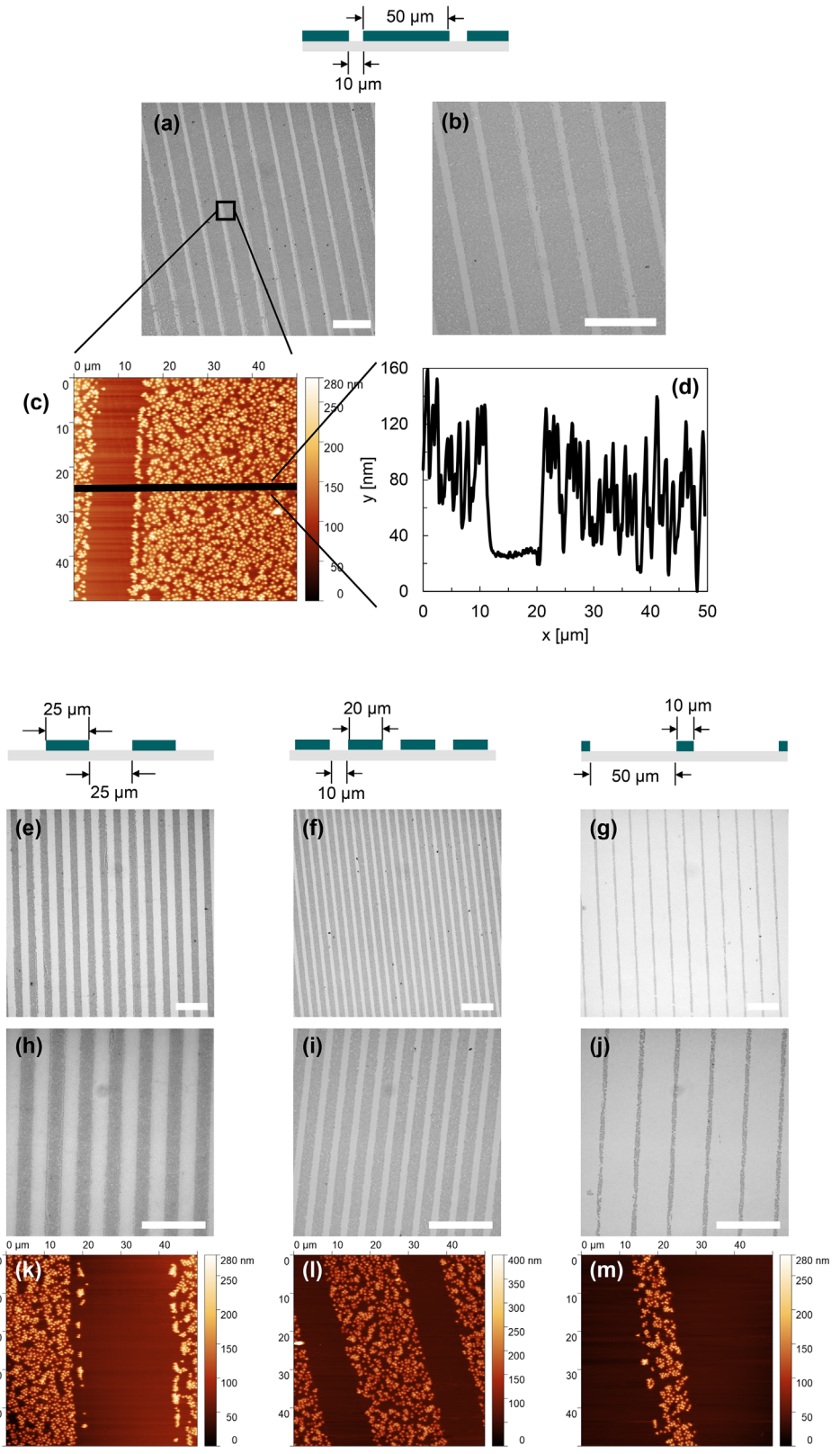

Figure 3. Imaging of surfaces structured with p(VCL-*co*-10mol%GMA-shell) microgels via microcontact printing. a,b,e-j) Light microscopy images and c,k-m) AFM images were recorded. Additionally, d) shows a height profile generated from the AFM image b). The ideal dimensions of resulting patterns are given in the schemes above. Dark grey areas in light microscopy images represent microgel stripes, lighter areas represent the bare glass. Scale bars in light microscopy images: 100 µm.

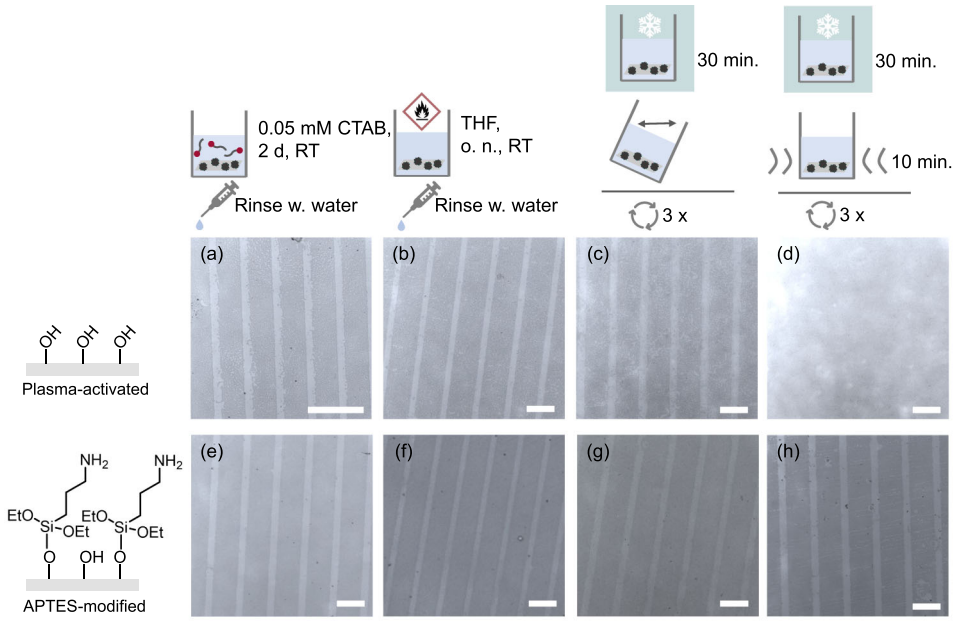

Figure 4. Stability tests of microgel patterns on a-d) plasma-activated and e-h) amine-modified substrates. Light microscopy images show patterned substrates, which were immersed in a,e) 0.05 mM CTAB solution for 2 d at room temperature, b,f) THF overnight at room temperature, c,g) 5 °C water for 30 min. with subsequent careful agitation for 30 min, or d,h) 5 °C water 30 min and subsequently sonicated for 10 min. Immersion and subsequent sonication/agitation cycle were repeated three times. Pattern: 50 µm microgel stripe, 10 µm spacer. Sufficient differences between the covalently attached and adhered microgels were found only for samples which were treated with cold water and ultrasonication. Scale bars are 100 µm.

2.3. Generation of Surface Chemical Gradients via Dip-Coating

Chemotaxis is relevant for the control of many biological processes[37] and biochemical gradients have been discussed as essential for the beginning of life itself. Surface gradients of peptides were created by various methods like controlled mixing of functional and unfunctional matrix building blocks,[7] exposing surfaces to concentration profiles through specialized vapor deposition techniques[9] or even controlled gradual cleavage of a functional group.[8] In our case, we want to employ the reactive glycidyl methacrylate (GMA) comonomer in p(VCL-*co*-10mol%GMA-shell) microgels. As shown in the supporting data (section S3), the epoxy moieties can successfully be post-modified with a variety of model nucleophiles in dispersion. However, to facilitate easy analysis, a reactive fluorescent dye, namely Cy3 amine, was chosen to explore the reaction kinetics in dispersion. Results in Figure S4.1 (Supporting Information) show that the coupling degree followed a saturation curve. In the beginning, many surface epoxy groups are readily available for reaction leading to a steep linear increase in fluorescence intensity within the first 2–4 h. Fluorescence intensity increases slower and reaches an upper limit after ≈6 h. The reaction, which may otherwise be completed within minutes,[38] could be slowed down in our system due to two potential reasons: First, both reactants (Cy3 amine and microgel) are significantly diluted in water. Second, a bulk of the epoxy moieties might be more difficult to access due to localization within the more hydrophobic GMA domains.

We hypothesized that the observed time-dependent increase of coupling degree could be harnessed to generate surface-chemical gradients by exposing different sections of a microgel-coated glass slide to a Cy3-solution for different durations. Such conditions can be realized by slowly immersing the sample with a micrometer dip-coater at a controlled speed. By choosing different immersion speeds, which eventually influences the exposure time of each section, a control of gradient steepness is expected. A scheme of how the structured substrates were slowly immersed into a Cy3 amine solution along the direction of stripes to generate the gradients is given in **Figure** 5a. Excess Cy3 amine solution was removed by carefully rinsing the substrates with *i*-propanol and water repetitively. Knowing the size of the coated substrate, a suitable immersion speed was chosen based on the kinetic experiments (Figure S4.1, Supporting Information). Since a saturation of the fluorescence intensity was evident from a reaction time of 6 h (at a Cy3 amine concentration of 2.3 µmol L^{-1}) with a linear increase up to 4 h, a maximum reaction times of 4–5 h was chosen for the surface modifications. For a sample size of 15 mm, this corresponds to a minimum immersion speed of 1 µm s^{-1}. A reference concentration of Cy3 amine (2.3 µmol L^{-1}) was adopted from the experiment in dispersion as well. In contrast to the reaction in dispersion, here, the dye solution was not agitated to avoid splashing and ensure uniform immersion conditions along the x axis. Only "passive" mixing might occur due to the immersion of the glass substrate.

Fluorescence microscopy images of different sections along the y-axis for a sample dip-coated at a concentration of 2.3 µmol L^{-1} and dipping speed of 1 µm s^{-1} are given in Figure 5b. The evaluation of fluorescence intensity was done with the surface plot function of the software *ImageJ*, shown in Figure 5c. The values were normalized in reference to the highest detected brightness for all samples. Intensity within the sections is lowest in the 10 µm spacer region. Broadening of the spacer may have occurred partially due to smudging during the printing procedure.

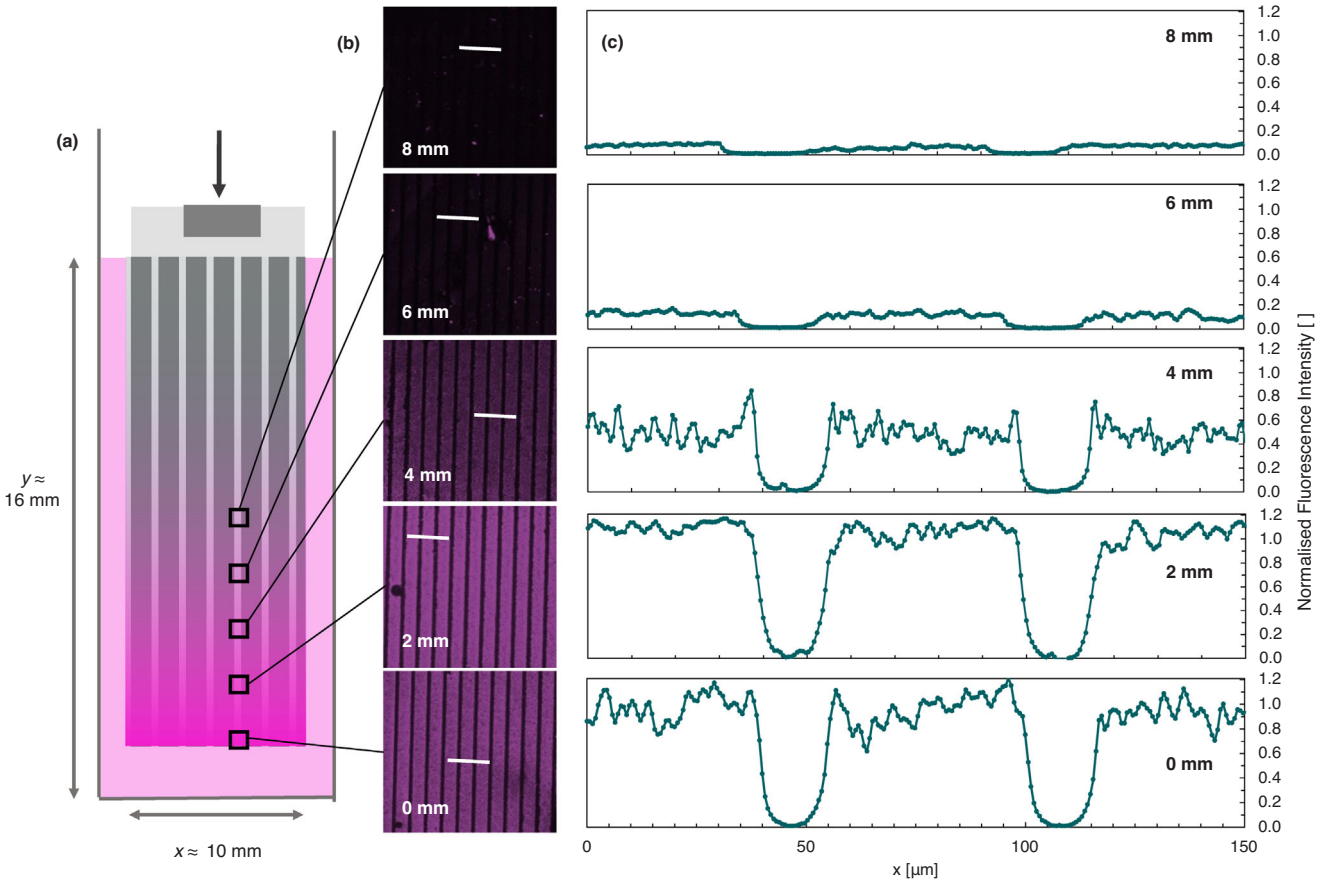

Figure 5. Gradients of Cy3 amine on a micro-patterned surface. a) Scheme of dip-coating procedure. b) Fluorescence microscopy images of a representative sample modified in a 2.3 µmol L^{-1} Cy3 amine solution at a dipping speed of 1 µm s^{-1}. Images were acquired with 8 s illumination time each at different positions along the y-axis. Fluorescence images were acquired with a laser of an excitation wavelength of 550 nm at 25% power and 8 s exposure time. White bars (150 µm) represent the plotted sections. c) Surface plots of marked sections.

Furthermore, it has to be noted that the intensity is not ideally homogeneous within the microgel stripes. As it was shown in AFM images of microgels monolayers, the microgels are not densely packed. Hence, the fluorescence intensity is lower between the microgels. The section at 0 mm was immersed first and was in contact with the Cy3 amine solution for ≈4.5 h. The section in image Figure 5b at a y-position of ≈8 mm was in contact with the Cy3 amine solution for ≈2 h. As expected, the brightness of the fluorescence decreases from 08 mm.

Two different Cy3 amine concentrations and three dipping speeds were applied to investigate their influence on the surface chemical gradient formation. The respective results are shown in **Figure 6**. All surfaces exhibit gradient formation with a fluorescence intensity decreasing from the side, which was first immersed to the other end along the y-axis (Figure 6a). However, the intensity decrease is not constant for all applied conditions. The maximum intensity of all samples prepared with the same Cy3 amine concentration and different immersion speeds is found for the slowest immersion speed of 1 µm s^{-1}. While the decrease is approximately linear within the error range for 2 and 3 µm s^{-1}, the gradient formed with 2.3 µmol L^{-1} at 1 µm s^{-1} appears to be more exponential.

Plotting the fluorescence intensity against the immersion time instead of the position along the y-axis allows for a better analysis and understanding of the observed effects (Figure 6b). Following the saturating increase of fluorescence intensity with reaction time in dispersion depicted in Figure S4.1 (Supporting Information), it is expected that there will be a larger difference in fluorescence intensity at y = 14 and 16 mm than y = 0 and 2 mm on the surface. Even though the difference in immersion time is ≈30 min for all positions that are 2 mm apart (at an immersion speed of 1 µm s^{-1}), microgels at y = 0 mm are exposed to the reagent for 4.5 h longer than the surface at y = 16 mm. It becomes apparent that sections which were immersed for the same duration (but at different immersion speeds) do not exhibit the same fluorescence intensity. That means that the modification degree is not only determined by the reaction time.

One potential explanation for the steep intensity increase at long reaction times for an immersion speed of 1 µm s^{-1} might be that the first surface increment at y = 0 mm always comes into contact with new solution volume increments containing unreached Cy3 amine at an initial concentration of 2.3 µmol L^{-1} first. For slower dipping speeds, the contact time for this first surface increment is longer and, thus, higher functionalization

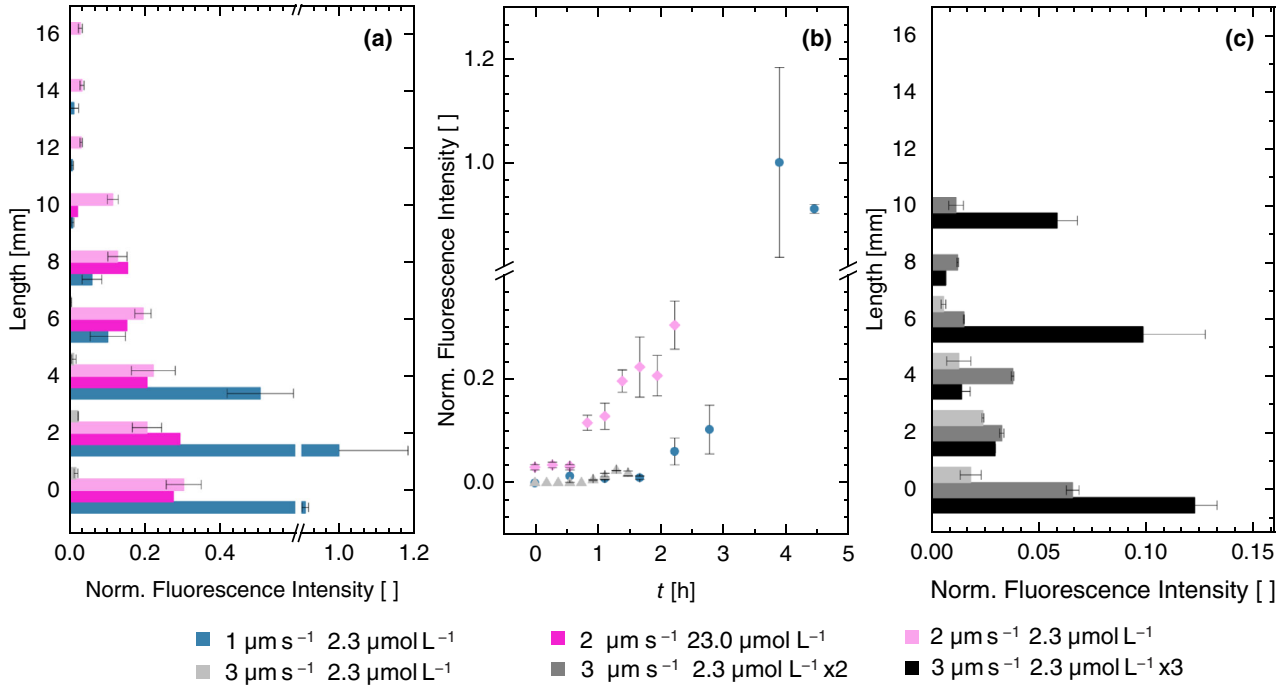

Figure 6. a,c) Normalized mean fluorescence intensities measured along y-axis of microgel-coated glass slides modified with Cy3 amine via dip-coating. b) The normalized fluorescence intensities of selected samples were also plotted against the immersion times calculated via the sample length and immersion speed. Samples were immersed in Cy3 amine solution at a concentration of 2.3 µmol L^{-1} at a speed of 1 µm s^{-1} (blue), 2 µm s^{-1} (shades of pink), and 3 µm s^{-1} (black/grey). The sample immersed at a speed of 3 µm s^{-1} was coated three times under the same conditions and analyzed each time. The respective evaluated images were acquired with a laser of an excitation wavelength of 550 nm at 25% power and 8 s exposure time. Error bars: mean ± standard deviation from a minimum of $n = 250$ data points at the same position along the y-axis.

degrees are reached. However, this leaves all solution increments, through which surface increments have already passed, with a lower remaining Cy3 amine concentration than at higher dipping speeds. Hence, the following surface increments (y > 0 mm) exhibit lower functionalization degrees at equal contact times but slower dipping speeds. In conclusion, the trends shown in panel Figure 6b allow for the assumption that the functionalization of surface immobilized p(VCL-*co*-10mol%GMA-shell) microgels with Cy3 amine is diffusion limited as new Cy3 amine needs to diffuse to the surface of the microgel and into the potentially slightly more shielded epoxy groups within the GMA domains for a maximum modification degree. This hypothesis is supported by a control experiment where separate microgel structured substrates were immersed for 4.4, 3.3 and 2.8 h respectively, which corresponds to the three latest time points for the immersion speed of 1 µm s^{-1}. The detected fluorescence intensity was the same for all three immersion times and significantly lower than the respective detected values for the dip-coated sample (Figure S5.1, Supporting Information).

The correlation of reaction time and fluorescence intensity was explored further by repeating the immersion process for the sample at 3 µm s^{-1} under the same reaction conditions and analyzing the fluorescent gradient each time Figure 6c. It should be noted that independent of the cycle number, the fluorescence intensities of all three samples are below the detection limit for distances ≥12 mm. Looking at specific sections along y- axis, it is possible to increase the mean fluorescence by immersing the sample multiple times, which is equivalent to increasing the reaction time. Samples which were immersed twice show higher fluorescence compared to a single immersion. However, the increase is not linear, meaning that doubling the reaction time does not simply result in a doubling of intensity. For a triple immersion, the fluorescence intensity fluctuates. Potential reasons for this might be that the molecules need to penetrate the microgels to reach the GMA domains all over again for each cycle, since samples are rinsed and dried in between. It also has to be noted, that some epoxy groups might hydrolyze without undergoing a reaction with the primary amine and hence will not available for further functionalization. Furthermore, surface contamination due to sample handling in between the cycles might hinder diffusion into parts of the sample, or partial bleaching after the imaging steps could explain the counterintuitive observations. Results again indicate that the correlation of reaction time and fluorescence intensity is complex and does not fully mirror the reaction behavior in dispersion, which is to be expected since both diffusion and fluid dynamic process can play a role. In summary, glass surfaces patterned with p(VCL-*co*-10mol%GMA-shell) microgels were successfully modified with Cy3 amine gradients via dip-coating. The gradient profiles were successfully controlled by changing the immersion speed.

2.4. RGD-Modified Patterns Impact Focal Adhesion Formation, Cell Morphology, and Directional Cell Motility

Promising results regarding pattern stability and successful post-modification including surface gradient formation with Cy3

amine and coupling in dispersion with a thiol containing RGD peptide sequence (Section S3, Supporting Information) motivate a proof-of-concept application of the developed platform in tissue culture. When working toward a more complex tissue culture set-up, e.g., involving the co-culture of different cell-types, a control over cell localization, especially with distinction toward the substrate background is desirable. This can be realized by equipping the surface features with cell adhesive peptides.

Chemical gradients alone proved to be strong enough to promote cell alignment[7,9] and provoked cells to respond with variations in density[8] and size[10] depending on the peptide concentration. However, control over the spatial distribution on distinct surface features, in our case guiding their localization on microgel stripes, is desirable. It is especially important for future adaptation of the system, when mechanical and biological signals of the patterns are to be adjusted to a certain cell type or a cargo should be released, cells need to specifically locate on top of the surface feature opposed to previously reported systems.[28,39]

NIH-3T3 cells were chosen for this study due to their efficient adhesion and movement on microgel patterns. Furthermore, because of the similarity in size between the cells and the microgel pattern geometries, single cells typically adhered to and moved along a single printed line. Micrometer-sized patterns minimize interactions with adjacent printed structures or the underlying substrate that could potentially alter cell behavior making its subsequent analysis more complex. This presents a clear advantage over previous work, where cells grown on sub-micrometer range p(NIPAm) microgel line patterns adhered to and moved along multiple adjacent linear patterns.[29,30] To this end, a thiol containing RGD peptide sequence was applied to functionalize the microgel patterned substrates. As a first proof of concept, cells were not seeded on RGD gradients but instead, only one side of a patterned substrate was exposed to the peptide for 15 h ensuring complete reaction. Such a sample effectively represents the two extremes of a gradient – no functionalization and maximum functionalization.

Results for statistical focal adhesion analysis (a-d) and representative live images (e,f) are shown in **Figure 7**. Cells were initially seeded in serum-free medium to analyze their interaction with the surface through the number and size area of focal adhesions (FAs). This eliminates the masking and confounding effect caused by adsorption of serum proteins on the functional surface. The static features of the focal adhesions were analyzed 24 h after seeding. Cells adhering on the RGD-modified part of the substrate clearly formed more focal adhesions resulting in both a larger total focal adhesion area per cell (Figure 7a) and a higher number of focal adhesions (Figure 7b). The mean total FA size is about 72 μm^2, which is almost double the size of FA formed on unmodified areas. As expected, when microgel patterns were modified with a scrambled RGD peptide, the statics properties of FA did not significantly differ from those of FA formed on uncoated patterns (Figure 7a–d). These observations are in good agreement with the work of Lagunas et al. showing a threefold increase in the number of focal adhesions per cell when comparing an area of high RGD-concentration to an area of low concentration along a gradient.[8] The explanation for the significantly higher number of FAs on the RGD-modified (45 on average in our experiments) compared to the work of Lagunas might lie in the type and surface concentration of the used sequence.

Next, cells were studied with live cell imaging to visualize their behavior on modified and unmodified areas of the substrate. Since live cell imaging required a 24-h longer experimental design, the serum-free medium was replaced with medium containing serum prior to starting the imaging experiments. To minimize potential experimental differences between imaging sessions, thiol-RGD modified and unmodified areas were prepared and analyzed on the same substrate. This ensures that all observed differences in cell behavior are exclusively due to the different chemical functionalization of the substrate sides. Moreover, cells attached to areas at the interface between coated and uncoated patterns were excluded from the analysis to minimize "mixed" cell behavior. Cells on RGD-modified microgel stripes (Video S2, Supporting Information; Figure 7e) preferably moved on the lines rather than the underlying APTES-functionalized glass substrates and acquired an elongated morphology along the line pattern. By contrast, cells on the unmodified substrate moved across multiple adjacent lines without acquiring an elongated morphology (Video S1, Supporting Information; Figure 7f).

In conclusion, post-modifying microgel patterned surfaces with RGD enables enhanced control over the adhesion and motility of cells. The exploration of this system is paving the way to design complex systems adapted to the needs of different cell types eventually enabling the study of multi-facetted processes like wound healing or tissue regeneration processes and the design of implantable devices.

3. Conclusion

Equipping otherwise flat and mostly inert surfaces with topographical cues and adaptable chemical functionalities is interesting for a variety of applications where properties of a bulk material do not comply with demands for its interface. One field, where this is especially critical, concerns biomedical applications, since cells have shown to respond to a multitude of chemical, mechanical, topographic, or electrical cues. The present study shows that such multifunctional surfaces can be generated by employing reactive microgels. Through microcontact printing, poly(*N*-vinylcaprolactam-*co*-glycidyl methacrylate) microgels could be structured in micrometer-sized line patterns onto glass substrates. Line patterns in the range of 10–50 µm appeared to be homogenous and proved to be stable on amine-functionalized glass withstanding rigorous washing due to binding of the reactive epoxy groups. These reactive groups could be furthermore employed for chemical post-modification with a fluorescent model compound baring a primary amine moiety. By making use of gradually changing contact times, fluorescent surface chemical gradients were generated by dipcoating the structured substrates. Gradient profiles could be adjusted through the dipping speed. Finally, multifunctional microgel-based substrates were exploited to modulate the motility and adhesion of NIH-3T3 cells. The binding of RGD peptides to microgel patterns enabled the substrates to promote cell adhesion (i.e., increase of FA formation) as well as directional cell motility. The adaptable, multifunctional surfaces made up of flexible colloidal building blocks described in this study are expected to be the substrate of reference for applications

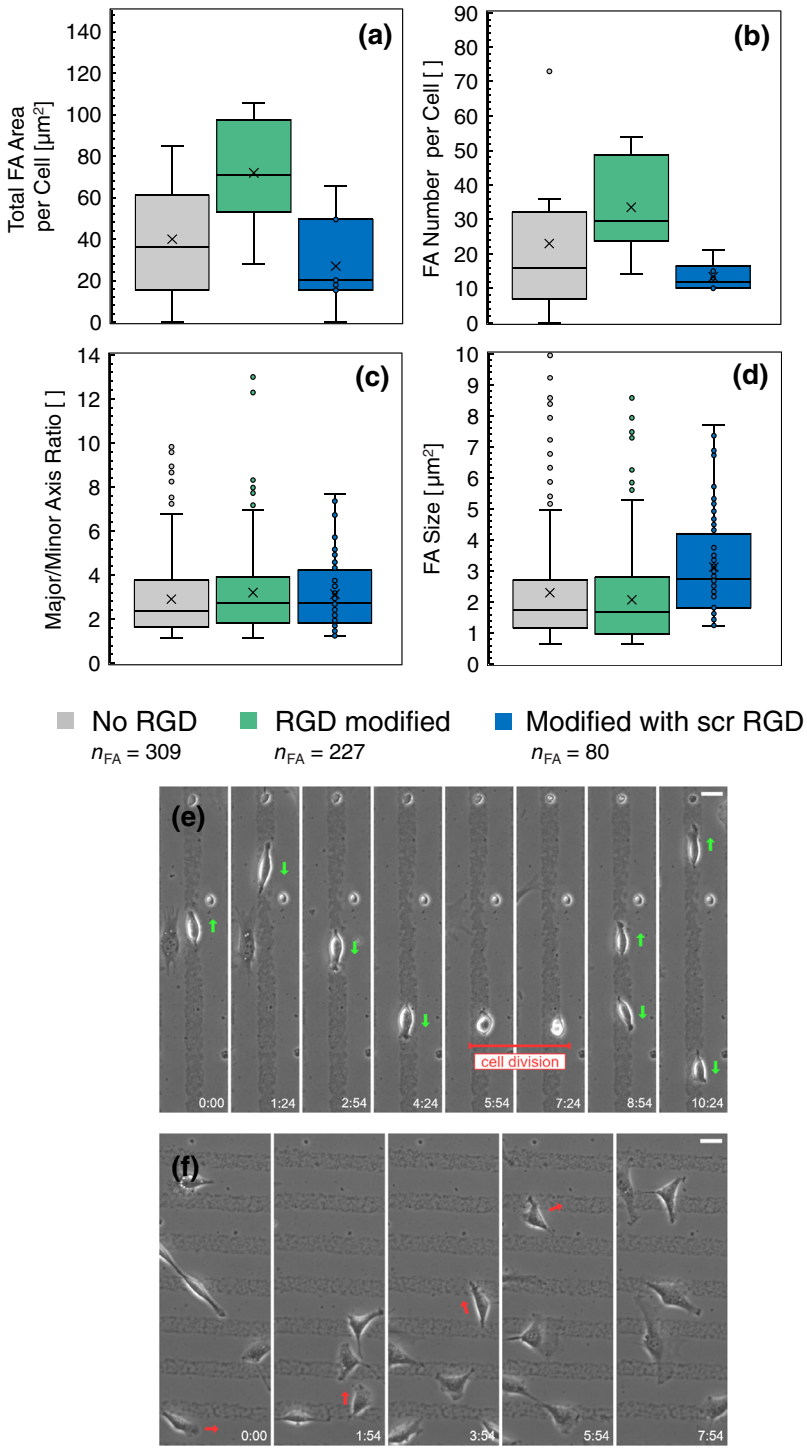

Figure 7. Statistical evaluation of a) focal adhesion (FA) number, b) area per cell c) major/minor axis ratio, and d) average size, which were assembled by NIH-3T3 cells seeded on the structured substrates. The samples were incubated in DMEM for 24 h without addition of the growth factor FCS, followed by fixation and staining. Imaging of focal adhesions was done at a gain of 300, with an excitation wavelength of 574–599 nm and at an exposure time of 100 ms. The medians are indicated as horizontal lines, the mean values are marked with a cross (x) and outliers by open circles (°). Upper and lower quartile correspond to the box edge. Whiskers indicate the maximum or minimum excluding outliers, which are defined as any data points that fall beyond 1.5 times the interquartile range above the upper quartile or below the lower quartile. Live imaging was performed for selected samples to evaluate the influence of RGD modification on cell motility. Representative phase contrast images from either e) the RGD-modified side or f) the unmodified side of the sample are shown. Scale bars: 25 µm. Cells on RGD-modified microgel stripes showed more and larger focal adhesions as well as a stronger preference of moving on RGD-coated lines over the underlying APTES-functionalized glass substrates as well as a robust elongated morphology. Conversely, cells on the unmodified substrate part moved across multiple adjacent lines without showing acquiring an elongated morphology.

requiring the modulation of growth, adhesion, and migration of cells particularly in the case of complex biological system such as multicellular assemblies and engineered tissues. They represent an interesting platform to investigate and understand processes such as wound healing and tissue formation.

4. Experimental Section

Materials: (3-Aminopropyl)triethoxysilane (APTES, 97%), 2,2′-azobis(2-methylpropionamidine) dihydrochloride (AMPA, 97%), bovine serum albumin (BSA, ≥96%), ethanol (99.8%), glycidyl methacrylate (GMA, ≥97.0%), *N*,*N*′-methylenebis(acrylamide) (BIS, 99%), paraformaldehyde (PFA, 95%), tetrahydrofuran (THF, 99%), Trizma buffer substance pH 8, tris(2-carboxyethyl)phosphine hydrochloride (TCEP, ≥98.0%), sodiumbicarbonate ($NaHCO_3$, ≥99.7%), sodium carbonate (Na_2CO_3, ≥ 99.0%), and *N*-vinylcaprolactam (VCL, 98%) were purchased from *Sigma–Aldrich*.

N-heptane (99%) and phosphate-buffered saline (PBS, 1X, sterile filtered) were acquired from *Fisher Scientific*. Cyanine3 amine (Cy3 amine, 95%) was provided by *Lumiprobe*. The peptide sequences (Acetyl-Cys-Doa*-Doa-Gly-Arg-Gly-Asp-Ser-Pro-NH2 and Acetyl-Cys-Doa*-Doa-Gly-Arg-Asp-Gly-Ser-Pro-NH2) were purchased from *Cellendes*. Furthermore, goat anti-mouse IgG (H+L) cross-adsorbed secondary antibody conjugated with Alexa Fluor (AF 647 GAM) and 4′,6-diamidino-2-phenylindole dihydrochloride by *Invitrogen*, as well as PH488 by *Proteintech* were applied. The stabilizer was removed from both monomers (VCL and GMA) via distillation. VCL was furthermore recrystallized in heptane. Poly(dimethylsiloxane) (PDMS) stamps were made from a Sylgard 184 Elastomer kit by *Dow Corning*. The used water, unless specified otherwise, was of HPLC grade, provided by *Merck Millipore*.

Microgel Synthesis and Characterization: The functional p(VCL-*co*-10mol%GMA-shell) microgel was synthesized via precipitation polymerization. The addition of the comonomer was delayed to achieve GMA-localization in the microgel shell. BIS (16.2 mg, 0.105 mmol, 2.0 mol%) and VCL (641.0 mg, 4.605 mmol, 87.4 mol%) were added to 50 mL of water, heated to 70 °C, and stirred at 250 rpm for ≈1 h with a constant nitrogen flow above the solution. The reaction was initiated by injecting AMPA (8.6 mg, 0.032 mmol, 0.6 mol%) dissolved in 1 mL of water into the stirred reaction dispersion. The comonomer GMA (72 µL, 0.527 mmol, 10 mol%) was added 3 min. after initiation. The reaction was terminated after 30 min. by transferring the hot dispersion into a dialysis tube (molecular weight cut-off 12–14 kg mol^{-1}). Microgels were dialyzed in de-ionized water for 7 days.

The synthesized microgel was characterized by dynamic light scattering (DLS) with a *Zetasizer Ultra* by *Malvern* to determine its temperature-responsiveness and monodispersity. Data points are presented as the mean value of three measurements and error bars of the hydrodynamic diameter (D_H), polydispersity (*PDI*) or zetapotential (ζ) represent the standard deviation. D_H and *PDI* were measured in a polystyrene cuvette between 15 and 50 °C in with the detector positioned at 90°. 2 °C steps with 120 s of equilibration time were used in the heating cycle (red dots) and 5 °C steps with 180 s of equilibration time in the cooling cycle (in turquoise dots). The zeta potential was measured in a DTS1070 cuvette with 120 s equilibration time each. Surface-coated microgels were imaged with atomic force microscopy on a *NanoScope V* AFM by *Veeco Instruments* in tapping mode. The *NCH-50 POINTPROBE-Silicon SPM-Sensor* cantilever was manufactured by *Nanoworld* and had a resonance frequency of 320 kHz and a force constant of 42 N m^{-1}. Images were evaluated in *Gwyddion* 2.67.

Surface Patterning and Stability: Glass substrates were cleaned consecutively in acetone, water, and *i*-propanol in an ultrasonic bath. Before use, the substrates were dried with compressed air. Hydrophilic substrates were prepared by treating the clean glass-slides with air-plasma for 180 s with a *Flecto10USB-MFC* plasma etcher by *Plasma Technology*. The amine-functionalized substrates were prepared by soaking cleaned substrates in 10 vol% APTES in ethanol for 2 h. Substrates were rinsed in ethanol repetitively to remove excess reactant and cured at 80 °C overnight.

Even microgel monolayers were created at the surfaces depending on the substrate size. Small, square glass slides and PDMS stamps (1 × 1 cm) were spin-coated with 50 µL of the microgel dispersion (1.2 wt.%) at 2000 rpm for 1 min on a WS-650SZ-6NPP/LITE by *Laurell*. Large stamps (as used for gradient production) were coated on a PTL-UMB dip-coater (*MTI Corporation*). The stamps were immersed in a 0.25 wt.% microgel dispersion for 30 min. and then slowly withdrawn at 10 µm s^{-1}.

Two different approaches were chosen for structuring the hydrophilic glass and the amino-silane functionalized glass. Plasma-activated glass was treated with a "reverse printing" procedure as described by Peng et al.[31] PDMS stamps were activated with air-plasma for 60 s and cooled for ≈15 min. at −20 °C before use. The hydrophilic substrates were pre-treated and coated with microgel as described above. The cooled stamps were contacted with the substrates for ≈5 s and carefully removed afterwards yielding the negative of the stamp pattern. Similarly, the amine-functionalized substrates were patterned with an adapted "direct structuring" method (shown in **Scheme 1**), where the substrates were cooled and PDMS stamps were coated with the microgel (instead of the substrate) to generate covalently bound structures. Substrate and stamp were contacted for ≈5 s yielding the positive pattern of the stamp.

Hydrophilic plasma-treated as well as APTES-modified glass substrates with microgel patterns (50 µm microgel stripe, 10 µm spacer) were both treated equally to test the pattern stability. Both structured surface types were immersed in 0.05 mM CTAB solution for 2 d at room temperature and THF overnight at room temperature. They were then immersed in 5 °C water for 30 min. and subsequently agitated carefully for 30 min. This process was repeated 3 times. A similar treatment with cold water was repeated, but instead the samples were sonicated for 10 min. After air-drying the substrates were imaged with light microscopy.

Light, Fluorescence, and Atomic Force Microcopy Imaging of Printed Structures: An *Axioplan 2* reflection microscope (*Carl Zeiss*) equipped with an *AxioCam MRc* camera was used to analyze the quality of structured substrates. An *AxioObserver Z1*, equipped with an *ApoTome* system, was used for imaging the Cy3 amine gradients. The laser was set at a wavelength of 550 nm with 25% power, and samples were illuminated for 8 s. Light and fluorescence microscopy images were evaluated with *ImageJ 15.4 g*.

50 × 50 µm scans of microgel patterned substrates were acquired on a *NanoScope V* AFM by *Veeco Instruments* in tapping mode. The applied cantilevers (*NCH-50 POINTPROBE-Silicon SPM-Sensor*, *Nanoworld*) had a resonance frequency of 320 kHz and a force constant of 42 N m^{-1}. *Gwyddion 2.67* was used for image evaluation.

Surface Chemical Gradients with Cy3 amine: Microstructured substrates (≈1 × 3 cm) were dip-coated with a *PTL-UMB* device (*MTI Corporation*). To modify the substrates with Cy3 amine, they were gradually immersed into the reaction solution at varying speeds and concentrations of Cy3 amine in carbonate buffer (50 mM, pH 10). After finished immersion, the substrates were immediately removed from the Cy3 amine solutions, extensively rinsed with i-propanol and water, and air dried. Samples were imaged with a *Zeiss Observer Z1* equipped with a *Colibri LED* light source at an excitation wavelength of 550 nm for 8 s (25%). Images were acquired at multiple positions along the y-axis of the sample using the same settings to allow for comparison of the fluorescence intensity. Normalized mean fluorescence intensities were evaluated by analyzing the images with *ImageJ 1.54g* using the surface plot function.

Peptide-Modified Substrates: The procedure to modify surfaces with peptides is schematically shown in **Scheme 2**. Here, a thiol-RGD modified and unmodified area were prepared on the same substrate to ensure optimal comparability of cultivation conditions for the live imaging experiments. One half of a microgel-patterned substrate was immersed in TRIS buffer (2.5 mL, 50 mM, pH8) containing the RGD peptide sequence Acetyl-Cys-Doa*-Doa-Gly-Arg-Gly-Asp-Ser-Pro-NH2 at a final concentration of 0.4 mM with a sixfold excess of tris(2-carboxyethyl)phosphine (TCEP) in respect to the peptide. The scrambled RGD sequence Acetyl-Cys-Doa*-Doa-

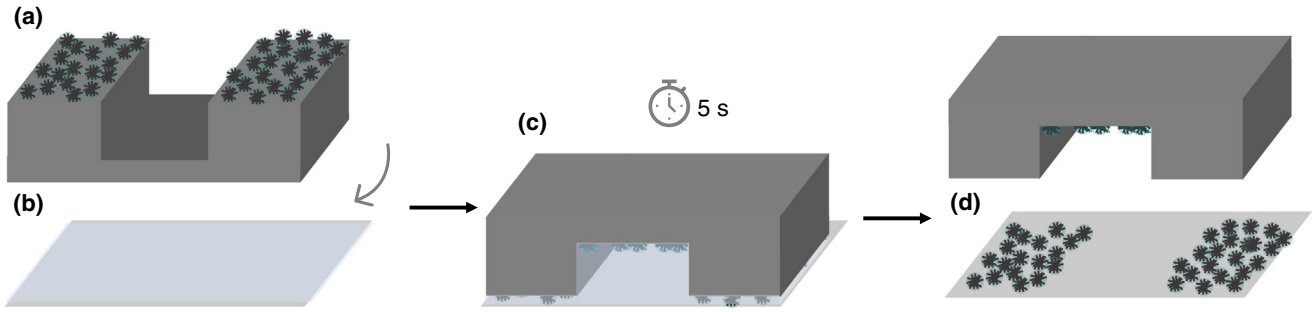

Scheme 1. Schematic representation of "direct micro-structuring method" adapted from Peng et al.[31] for covalently bound patterns. Adversely to the original method, microgels are a) coated onto PDMS stamp (instead of the substrate) and b) water is condensed on the cold functionalized glass substrate (instead of the PDMS stamp). Similarly to Peng et al.,[31] c) stamp and surface are then contacted. d) The resulting pattern upon stamp removal in this adapted method, however, is representing the stamp pattern (instead of the negative pattern).

Gly-Arg-Asp-Gly-Ser-Pro-NH2 was used for reference experiments. The solution was mixed for 10 min. at RT prior to use. After 15 h of immersion time under mild agitation on a rocker shaker, all substrates were extensively rinsed with TRIS-buffer (50 mM, pH8), 1X PBS buffer and stored for no more than 1 h in 1X PBS at rt before application in tissue culture experiments.

Culture of NIH-3T3 Cells: NIH-3T3 mouse fibroblasts (ATCC, CRL-1658; RRID: CVCL_0594) were cultured in DMEM high glucose supplemented with 10% FCS, 2 mM *L*-glutamine, 100 µg mL^{-1} streptomycin and 100 U mL^{-1} penicillin at 37 °C, 5% CO_2.

Live Cell Imaging and Immunofluorescence Microscopy: To investigate cell motility, NIH-3T3 cells (6×10^5) were resuspended in a serum-free medium and then seeded onto structured surfaces. After 24 h, the structured substrates were transferred to a new dish containing a regular cell culture medium (i.e., with FCS). Images were acquired over a 24-h period (at 37 °C, 5% CO_2) using an *Axio Observer Z1* microscope (*Zeiss*) equipped with a *Plan-Apochromat* 10x objective and an *AxioCam MRm* (Zeiss) driven by Zen 2 software (*Zeiss*). Images were captured at 5-min intervals at various locations corresponding to well-defined printed structures using a motorized X-Y stage. Supplementary videos were assembled using *ImageJ*.

For the visualization of focal adhesions, cells were cultured on structured substrates in serum-free medium for 24 h before chemical fixation using 4% paraformaldehyde for 20 min. at RT and permeabilization with 0.1% Triton X-100 (in PBS) for 1 min. at RT. The actin cytoskeleton was labelled with Alexa 488-conjugated phalloidin (0.3 U mL^{-1}). Nuclei were labelled with the DAPI (5 µg mL^{-1}). Focal adhesions were labelled using an anti-vinculin antibody (1:400, hVin1) followed by Alexa 647-conjugated goat anti-mouse IgG (2 µg mL^{-1}). Images were acquired with an *Axio Observer Z1* microscope equipped with a *Evolve delta EM-CCD* camera driven by *Zen 2* software. Focal adhesions were imaged with an excitation wavelength of 574–599 nm, an exposure time of 100 ms, and at a gain of 300. Image processing and handling were done using the freeware programme *ImageJ* and *Affinity Photo* (ver. 2, Affinity, USA).

Analysis of Focal Adhesion Static Properties: The analysis of focal adhesions was done using the Focal Adhesion Analysis server created by Berginski et al.[40] Following the uploading of the images, the detection threshold was set for each individual image and a minimum adhesion size of 10 pixel and phase length of 3 were adjusted for better detection and segmentation of focal adhesions. The following focal adhesion static properties were finally calculated: number of focal adhesions per cell, size, elongation (ratio major to minor axis). The sample size of analyzed focal adhesions was 227 for the RGD treated sample, 309 for the sample without RGD and 80 for the reference, which was modified with scrambled RGD.

Statistical Analysis: Statistical data was processed and evaluated with *Microsoft Excel* for *Microsoft 365 Version 2507* and *OriginPro 2024b*. Mean values for the fluorescence intensity (Figure 6) and standard deviations were calculated for microgel stripe section with a minimum of 250 data points at the same y-position in one image. The mean fluorescence in the microgel stripe areas was subtracted from the mean fluorescence in the spacer area and data for different conditions (i.e., Cy3 amine concentration and immersion speed) was normalized to the highest measured intensity. DLS and ELS (Figure 2; Figure S3.2, Supporting Information) measurements were recorded in triplicate and data is presented as the mean value,

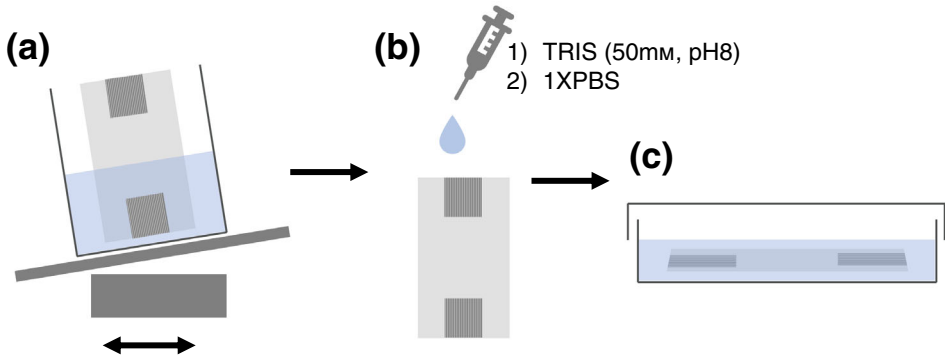

Scheme 2. Schematic representation of peptide modification of mocrogel-structured substrates for application in tissue culture. a) One half of a structured glass substrate is immersed in pH8 TRIS buffer (50 mM) containing the RGD peptide sequence at a final concentration of 0.4 mmol L^{-1}. The substrate is lightly agitated for 15 h. b) The entire substrate is extensively rinsed with TRIS buffer at pH8, followed by 1XPBS. c) The substrate is stored in 1XPBS buffer before application in tissue culture.

while the error bars correspond to the calculated standard deviation. For the analysis of focal adhesions (Figure 7), 2–3 independent experiments were analyzed for each condition (i.e., RGD, no RGD and scrambled RGD). In each experiment, a minimum of 80 focal adhesions were analyzed. Exact numbers are specified in the figure legend. The line in the middle of all box plots indicates the median, the bottom of the box indicates the 25th quartile, whereas the bottom of the box indicates the 75th quartile. The mean values are marked with a cross (x) and outliers by open circles (°). Outliers are defined as the data points that fall beyond 1.5 times the interquartile range above the upper quartile or below the lower quartile.

Supporting Information

Supporting Information is available from the Wiley Online Library or from the author.

Acknowledgements

The authors would like to thank Renate Jansen for conducting the ICP measurements. The authors sincerely appreciate the Deutsche Forschungsgemeinschaft (DFG) for funding the projects "Active photo-responsive microgel-structured surfaces for triggered particle movement" as well as the project "Adaptive Living Seed Coatings" within the Priority Program "Engineered Living Materials". DFG project "Active Photo-Responsive Microgel-Structured Surfaces for Triggered Particle Movement" (544907265) as well as the project "Adaptive Living Seed Coatings" (541298489) within the Priority Program "Engineered Living Materials".

Open access funding enabled and organized by Projekt DEAL.

Conflict of Interest

The authors declare no conflict of interest.

Author Contributions

I.L., A.T., M.Z., A.S., and A.P. conceived the project; I.L., A.T., A.S., M.Z., and A.P. designed the experiments; I.L. and A.S. performed experiments and data processing. All authors contributed to the analysis of the data and interpreted the results. The manuscript was written through the contribution of all authors. All authors have given approval to the final version of the manuscript.

Data Availability Statement

The data that support the findings of this study are available from the corresponding author upon reasonable request.

Keywords

microcontact printing, microgels, post-modification, surface-chemical gradient

Received: June 24, 2025
Revised: September 5, 2025
Published online:

[1] S. Rossi, G. Gai, R. de Benedetto, *Mater. Des.* **2014**, *53*, 782.
[2] H. Dodiuk, P. F. Rios, A. Dotan, S. Kenig, *Polym. Adv. Technol.* **2007**, *18*, 746.
[3] a) E. Schönemann, J. Koc, J. F. Karthäuser, O. Özcan, D. Schanzenbach, L. Schardt, A. Rosenhahn, A. Laschewsky, *Biomacromolecules* **2021**, *22*, 1494; b) I. Banerjee, R. C. Pangule, R. S. Kane, *Adv. Mater.* **2011**, *23*, 690.
[4] S. Cai, C. Wu, W. Yang, W. Liang, H. Yu, L. Liu, *Nanotechnol. Rev.* **2020**, *9*, 971.
[5] N. J. Sniadecki, R. A. Desai, S. A. Ruiz, C. S. Chen, *Ann. Biomed. Eng.* **2006**, *34*, 59.
[6] a) S. C. Hernández, C. J. C. Bennett, C. E. Junkermeier, S. D. Tsoi, F. J. Bezares, R. Stine, J. T. Robinson, E. H. Lock, D. R. Boris, B. D. Pate, J. D. Caldwell, T. L. Reinecke, P. E. Sheehan, S. G. Walton, *ACS Nano* **2013**, *7*, 4746; b) J. Genzer, *Annu. Rev. Mater. Res.* **2012**, *42*, 435.
[7] S. A. DeLong, A. S. Gobin, J. L. West, *J. Controlled Release* **2005**, *109*, 139.
[8] A. M. Ender, K. Kaygisiz, H.-J. Räder, F. J. Mayer, C. V. Synatschke, T. Weil, *ACS Biomater. Sci. Eng.* **2021**, *7*, 4798.
[9] C. M. Motta, K. J. Endres, C. Wesdemiotis, R. K. Willits, M. L. Becker, *Biomaterials* **2019**, *218*, 119335.
[10] A. Lagunas, J. Comelles, E. Martínez, E. Prats-Alfonso, G. A. Acosta, F. Albericio, J. Samitier, *Nanomed.: Nanotechnol., Biol. Med.* **2012**, *8*, 432.
[11] a) L. E. Dickinson, C. Lütgebaucks, D. M. Lewis, S. Gerecht, *Lab Chip* **2012**, *12*, 4244,; b) A. Kikuchi, T. Okano, *J. Controlled Release* **2005**, *101*, 69.
[12] J. L. Wilbur, A. Kumar, E. Kim, G. M. Whitesides, *Adv. Mater.* **1994**, *6*, 600.
[13] A. Brock, E. Chang, C.-C. Ho, P. LeDuc, X. Jiang, G. M. Whitesides, D. E. Ingber, *Langmuir* **2003**, *19*, 1611.
[14] C. K. Yeung, L. Lauer, A. Offenhäusser, W. Knoll, *Neurosci. Lett.* **2001**, *301*, 147.
[15] B. C. Wheeler, J. M. Corey, G. J. Brewer, D. W. Branch, *J. Biomech. Eng.* **1999**, *121*, 73.
[16] M. Nakayama, Y. Toyoshima, A. Kikuchi, T. Okano, *Macromol. Biosci.* **2020**, *21*, 2000330.
[17] I. A. Janson, A. J. Putnam, *J. Biomed. Mater. Res., Part A* **2015**, *103*, 1246.
[18] A. Pich, W. Richtering, *Advances in Polymer Science*, 1st ed., Springer, Berlin Heidelberg **2011**.
[19] A. Mourran, Y. Wu, R. A. Gumerov, A. A. Rudov, I. I. Potemkin, A. Pich, M. Möller, *Langmuir* **2016**, *32*, 723.
[20] C. C. Cutright, J. L. Harris, S. Ramesh, S. A. Khan, J. Genzer, S. Menegatti, *Adv. Funct. Mater.* **2021**, *31*, 2104164.
[21] E. Gau, D. M. Mate, Z. Zou, A. Oppermann, A. Töpel, F. Jakob, D. Wöll, U. Schwaneberg, A. Pich, *Biomacromolecules* **2017**, *18*, 2789.
[22] Z. Zou, E. Gau, I. El-Awaad, F. Jakob, A. Pich, U. Schwaneberg, *Bioconjugate Chem.* **2019**, *30*, 2859.
[23] a) G. Agrawal, R. Agrawal, A. Pich, *Part. Part. Syst. Charact.* **2017**, *34*, 1700132; b) M. Mackiewicz, S. Dagdelen, K. Marcisz, E. Waleka-Bargiel, Z. Stojek, M. Karbarz, *Polym. Degrad. Stab.* **2021**, *190*, 109652.
[24] a) X. He, H. Han, L. Liu, W. Shi, X. Lu, J. Dong, W.u Yang, X. Lu, *ACS Appl. Mater. Interfaces* **2019**, *11*, 13676; b) S. Della Shin, E. Y. Tokuda, J. L. Leight, C. E. Miksch, T. E. Brown, K. S. Anseth, *ACS Biomater. Sci. Eng.* **2018**, *4*, 378.
[25] a) A. W. Bridges, N. Singh, K. L. Burns, J. E. Babensee, L. Andrew Lyon, A. J. García, *Biomaterials* **2008**, *29*, 4605; b) M. Kather, M. Skischus, P. Kandt, A. Pich, G. Conrads, S. Neuss, *Angew. Chem. (International ed. in English)* **2017**, *56*, 2497.
[26] a) S. Schmidt, T. Hellweg, R. von Klitzing, *Langmuir* **2008**, *24*, 12595; b) S. Schmidt, M. Zeiser, T. Hellweg, C. Duschl, A. Fery, H. Möhwald, *Adv. Funct. Mater.* **2010**, *20*, 3235.

[27] K. Uhlig, T. Wegener, J. He, M. Zeiser, J. Bookhold, I. Dewald, N. Godino, M. Jaeger, T. Hellweg, A. Fery, C. Duschl, *Biomacromolecules* **2016**, *17*, 1110.
[28] Y. Xia, Y. Tang, H. Wu, J. Zhang, Z. Li, F. Pan, S. Wang, X. Wang, H. Xu, J. R. Lu, *ACS Appl. Mater. Interfaces* **2017**, *9*, 1255.
[29] A. Sechi, J. M. G. Freitas, P. Wünnemann, et al., *Adv. Mater. Interfaces* **2016**, *3*, 1600455.
[30] J. Riegert, A. Töpel, J. Schieren, R. Coryn, S. Dibenedetto, D. Braunmiller, K. Zajt, C. Schalla, S. Rütten, M. Zenke, A. Pich, A. Sechi, *PLoS One* **2021**, *16*, 0257495.
[31] J. Peng, D. Zhao, X. Tang, F. Tong, L.i Guan, Y. Wang, M. Zhang, T. Cao, *Langmuir* **2013**, *29*, 11809.
[32] N. Häntzschel, F. Zhang, F. Eckert, A. Pich, M. A. Winnik, *Langmuir* **2007**, *23*, 10793.
[33] C. E. Hoyle, A. B. Lowe, C. N. Bowman, *Chem. Soc. Rev.* **2010**, *39*, 1355.
[34] K. Nagase, H. Kuramochi, D. W. Grainger, H. Takahashi, *Mater. Today Bio.* **2025**, *32*, 101657.
[35] H. Takahashi, M. Nakayama, K. Itoga, M. Yamato, T. Okano, *Biomacromolecules* **2011**, *12*, 1414.
[36] E. Izak-Nau, D. E. Demco, S. Braun, C. Baumann, A. Pich, R. Göstl, *ACS Appl. Polym. Mater.* **2020**, *2*, 1682.
[37] H. E. Ives, F. C. Rector, *J. Clin. Invest.* **1984**, *73*, 285.
[38] R. M. Loureiro, T. C. Amarelo, S. P. Abuin, E. R. Soulé, R. J. Williams, *Thermochim. Acta* **2015**, *616*, 79.
[39] H.-Y. Tsai, K. Vats, M. Z. Yates, D. S. W. Benoit, *Langmuir* **2013**, *29*, 12183.
[40] M. E. Berginski, S. M. Gomez, *F1000Research* **2013**, *2*, 68.